JOM, Vol. 67, No. 1, 2015
DOI: 10.1007/s11837-014-1218-2

High Performance Oxides-Based Thermoelectric Materials

GUANGKUN REN,[1] JINLE LAN,[1] CHENGCHENG ZENG,[1] YAOCHUN LIU,[1] BIN ZHAN,[1] SAJID BUTT,[1] YUAN-HUA LIN,[1,2] and CE-WEN NAN[1,3]

1.—State Key Laboratory of New Ceramics and Fine Processing, School of Materials Science and Engineering, Tsinghua University, Beijing 100084, People's Republic of China. 2.—e-mail: linyh@tsinghua.edu.cn. 3.—e-mail: cwnan@tsinghua.edu.cn

Thermoelectric materials have attracted much attention due to their applications in waste-heat recovery, power generation, and solid state cooling. In comparison with thermoelectric alloys, oxide semiconductors, which are thermally and chemically stable in air at high temperature, are regarded as the candidates for high-temperature thermoelectric applications. However, their figure-of-merit ZT value has remained low, around 0.1–0.4 for more than 20 years. The poor performance in oxides is ascribed to the low electrical conductivity and high thermal conductivity. Since the electrical transport properties in these thermoelectric oxides are strongly correlated, it is difficult to improve both the thermoelectric power and electrical conductivity simultaneously by conventional methods. This review summarizes recent progresses on high-performance oxide-based thermoelectric bulk-materials including n-type ZnO, $SrTiO_3$, and In_2O_3, and p-type $Ca_3Co_4O_9$, BiCuSeO, and NiO, enhanced by heavy-element doping, band engineering and nanostructuring.

INTRODUCTION

Scientists worldwide have been working in recent years to help meet increasing energy demands with minimal environmental impact. Thermoelectric power generators directly convert temperature gradients and heat into electrical voltages and power, without the additional need for an electromechanical generator,[1] and up to now much interesting work has been focused on thermoelectric alloys such as Bi_2Te_3,[2] Mg_2Si[3] MnSi[4] and SiGe[5] because they have much better figure-of-merit values, ZT, compared with other materials. Most recently, for example, Zhao et al. have reported a ZT ~2.66 at 923 K realized in SnSe single crystals measured along the b axis of the room-temperature orthorhombic unit cell, which is the highest ZT for thermoelectric bulks until now.[6]

$ZT = S^2\sigma T/\kappa$ where S is Seebeck coefficient, σ electrical conductivity, κ thermal conductivity, and T absolute temperature, and high ZT requires high σ, low κ and relatively high S. Generally, it is difficult to achieve high ZT values due to the interdependency of the electronic terms (σ, S, and κ). For instance, an increase in σ leads to an increase in κ_e, through the Wiedemann–Franz law.

Even though the performances of most alloys are fascinating, they are usually toxic, low in abundance as natural resources, not environmentally friendly[7] and their thermal or chemical stability are inferior. Most of all, some of them can only be used in a strict oxygen-free environment. In contrast, oxide-based thermoelectric materials characterized with sufficient stability such as $Ca_3Co_4O_9$,[8] $CaMnO_3$,[9] $SrTiO_3$,[10] BiCuSeO,[11] ZnO,[12] In_2O_3[13] and NiO,[14] have been developed in recent years, and they are more suitable for high-temperature applications due to their structural and chemical stabilities, oxidation resistance, easy processing, and low cost.[15–19] Nevertheless, their ZT values are not high enough compared with those good thermoelectric alloys. Therefore, to find efficient ways to improve their electrical performance with stable low thermal conductivity is a promising strategy for oxide-based thermoelectric materials.

According to Ioffe's theory, oxide-based materials are not proper candidates for thermoelectric materials because they have ionic bonding with a narrow band when compared with covalent alloys. The

(Published online November 22, 2014)

carrier concentration and its mobility are two or three orders of magnitude lower than the covalent materials. Moreover, large bonding energies lead to a small atom mass of oxygen, which results in higher vibrational frequencies for crystals and consequently yields high lattice thermal conductivity. In 1997, Terasaki reported a Na_xCoO_2 crystal with a high $ZT \sim 1$, which leads to general electrical performance and low thermal conductivity.[20]

Moreover, thermopower, also defined as Seebeck coefficient S, is the most interesting and challenging functional parameter. From the basic equation ($ZT = S^2\sigma T/\kappa$) we confirm S is a quadratic parameter, and, to optimize S by efficient methods like band engineering would be more efficient for an improvement of ZT. The theory of irreversible thermodynamics combines S with transport coefficients by the equation:

$$S = -\frac{k_B}{e}\left(\frac{H}{T} - \frac{\mu_c}{T}\right) \quad (1)$$

where k_B is the Boltzmann constant, μ_c is the chemical potential, and H is the heat transporter particle, and for different materials, this formula can be deduced to some more applicable forms. As for oxide-based thermoelectric materials $\sigma = ne\mu$, this can be explained by the polaron hopping model.

In terms of thermal conductivity (κ), heat energy can be transferred by carrier (electrons and holes) and phonons. $\kappa = \kappa_e + \kappa_L$, κ_e is electronic thermal conductivity and κ_L is lattice thermal conductivity. κ_e depends on

$$\kappa_e = L\sigma T \quad (2)$$

where L is the Lorenz factor. Phonons are a quantum mode of vibration which play a key role because they are the primary means by which heat conduction takes place in solids. The lattice thermal conductivity, also known as phonon thermal conductivity, is more important than electronic thermal conductivity in most thermoelectric materials just because κ_e/κ_L is very small. High σ, low κ and relatively high S can be obtained by some appropriate methods. In this article, we will first review some progress concerning different oxide-based thermoelectric materials and then discuss how to enhance its power factor (PF) or figure-of-merit (ZT) by some appropriate strategies.

In order to obtain high ZT in the oxides-based semiconductors, high electrical conductivity and low thermal conductivity are desirable. However, the comodification of electrical properties (i.e., both high σ and S) is difficult, and, therefore, reducing the thermal conductivity is more attractive. Normally, κ in solids is governed by the lattice contribution (phonon vibrations) and the electronic component corresponding to the electron motions. For oxides, the phonon contribution remains the predominant component of the total thermal conductivity.[21] Strategies of lowering the lattice thermal conduction, i.e., enhancing the phonon scattering, include the application of nanostructures which affect the phonon mean free path, or the introduction of adding "impurity" atoms which serve as scattering centers. The thermal conduction in nanostructures can be dominated by the interface scattering of phonons and the associated thermal boundary resistance.

n-TYPE OXIDES-BASED THERMOELECTRIC MATERIALS

ZnO-Based Materials

As a candidate for use in thermoelectric applications,[22] zinc oxide (ZnO) has attracted attention for its high melting point, high electrical conductivity by Al-doping, and mediated Seebeck coefficient. Nevertheless, ZnO possess high lattice thermal conductivity due to its noncomplex wurtzite structure, which heavily limits the interest in ZnO for thermoelectric application. Hence, decreases in κ_L would directly lead to a decrease of κ and finally improve ZT.

Recently, many experimental efforts on structural effect have been made to improve the thermoelectric performance of ZnO pellets, as seen in Fig. 1. One of the effective methods is the introduction of a second nanophase. The major matrix and secondary minor phase must be chosen considering phase stability and compatibility. By utilizing natural phase separation and precise thermal treatment, the minor phase can be selectively induced to precipitate as nanoparticles. Attributed to plenty of interfaces and defects, enhanced phonon scattering promoted by Al-induced grain refinement and $ZnAl_2O_4$ nanoprecipitates presages a low κ of about 2 W m^{-1} K^{-1} and $ZT \sim 0.44$ at 1000 K.[12] Furthermore, Wu et al. have reported that the presence of polyparaphenylene (PPP) nanoparticles in the $Zn_{1-x}Ni_xO$ matrix is found to be effective in improving ZT by the dual effects of increased power factor consistent with the molecular junction effect and a reduction in thermal conductivity, and the maximum $ZT \sim 0.54$ is obtained as a result, which is sixfold higher than the $Zn_{0.97}Ni_{0.03}O$ sample fabricated by the same method.[24] The second way is to achieve excellent carrier transport properties in ZnO nanowires. Khanal and his coworkers suggest that the maximum electron concentration that can be achieved in ZnO nanowires with the diameter under 60 nm via doping method is 9×10^{19} cm^{-3}.[25] The electronic structures of ZnO nanowires doped with Al, Ga, and Sb elements are investigated by using first-principle calculations and the researchers noted that the electron effective masses of ZnO nanowires increase after being doped. These enhancements are mainly due to the interaction or admixture of host states and impurity states at the conduction band minimum. Based on the amphoteric defect model (ADM) and quantum confinement effects, Wang et al. found that the band gaps of ZnO nanowires doped with Al and Ga are narrowed, compared with that of undoped ZnO nanowires, and the maximum value of $ZT \sim 0.147$, is obtained for the Ga-doped sample.[26]

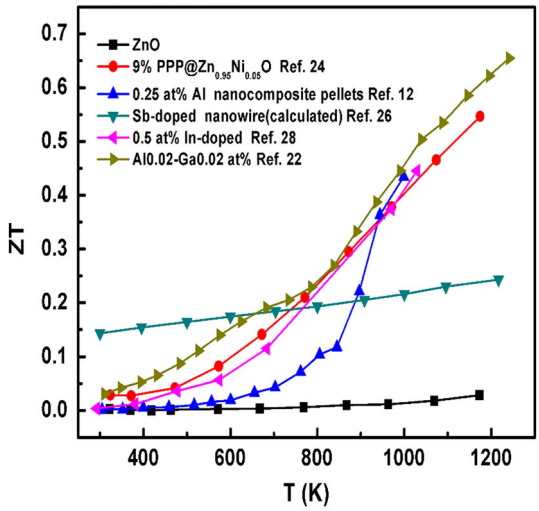

Fig. 1. Recent progress of thermoelectric figure-of-merit in ZnO.

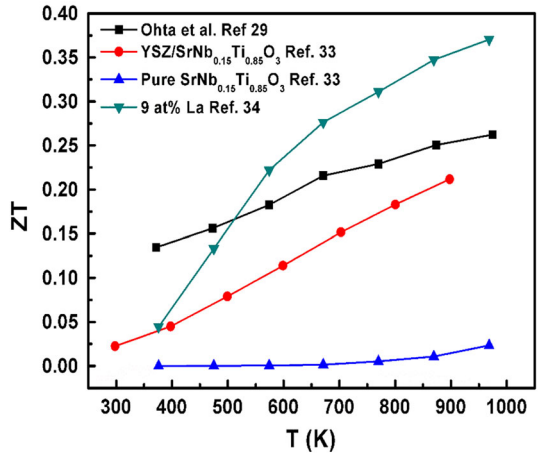

Fig. 2. Improving thermoelectric figure-of-merit (*ZT*) for STO.

In addition, nano-structured Al-doped ZnO with different morphologies is another way to improve *ZT*.[27] Li et al. synthesized ZnO, respectively, by the soft chemistry method and solid state reaction, and the measured *ZT* values along the preferred orientation directions were found to be 0.16 and 0.25 at 1223 K for the samples consolidated from rods and platelets, respectively. However, because the introduced grain boundary and nanoprecipitate scattering selectively depress the phonon spectrum, the sample consolidated from nanoparticles exhibited fine grains and highly distributed nanoprecipitates, resulting in a *ZT* value of 0.3 at 1223 K. After comparing the electrical conductivity with the Seebeck coefficient, they found the difference in electrical resistivity can be attributed to a variation in morphology rather than its composition, and the length scale of electron and phonon scattering is more effective in the nanostructural than in the microstructural range. Therefore, the discrepancy in the thermoelectric properties between the samples produced by the different synthesis methods is mainly caused by differences in defects and crystallinity, rather than the microstructural morphology. In addition, nanograins and carrier concentration refinement by high atomic number dopants and vitrified boundary are good ways to get high performance. *ZT* can be 0.45 at 1000 K by 0.5 at.% Indium doping.[28] Although Bi doping is not a good choice, much more effective phonon scattering by vitrified boundary through Bi segregation may be a new strategy for the future.

$SrTiO_3$-Based Materials

$SrTiO_3$ becomes a promising TE oxide as confirmed from the TE properties of $SrTiO_3$ single crystals.[10,29] Undoped $SrTiO_3$ is an insulator with no free electrons, but it becomes an *n*-type semiconductor and its metallic behavior appears upon doping with a small amount of La.[30] Electron-doped $SrTiO_3$ has a large *ZT* not only because of its relatively high electrical conductivity but also the large Seebeck coefficient induced by its high carrier mobility and large effective mass. A single crystal of bulk La-doped $SrTiO_3$ showed a high power factor of 28–36 mW cm^{-1} K^{-2} at room temperature,[10] which is comparable to the power factors of Bi_2Te_3 compounds. Although its *ZT* is less than 1 because of its large thermal conductivity, La-doped $SrTiO_3$ is one of the best *n*-type oxide thermoelectric materials (Fig. 2).

In 2007, Dresselhaus et al. proposed that nanocomposite thermoelectric materials would offer a promising approach for the preparation of bulk samples with nano-sized constituents.[31] The theoretical minimum κ, κ_{min}, which is derived from Cahill's model as follows, is ~1.4 W m^{-1} K^{-1} at 300 K and ~1.8 W m^{-1} K^{-1}at 1000 K for $SrTiO_3$.

$$\kappa_{\min} = \left(\frac{\pi}{6}\right)^{1/3} k_B N^{2/3} \sum_i v_i \left(\frac{T}{\theta_i}\right)^2 \int_0^{\theta_i/T} \frac{x^3 e^x}{(e^x-1)^2} dx \quad (3)$$

$$\theta_i = v_i(\hbar/k_B)\left(6\pi^2 N\right)^{1/3} \quad (4)$$

where k_B is the Boltzmann constant, $\hbar$ is the reduced Planck constant, *N* is the number density of atoms, and v_i is the sound velocities. Wang[32] has reported an effective path to increase the electrical conductivity while decreasing the thermal conductivity, and thus to enhance the *ZT* value by nano-inclusions. By this method, the *ZT* value of Nb-doped $SrTiO_3$ was enhanced by yttria-stabilized zirconia (YSZ) nano-inclusions (Fig. 3). YSZ inclusions, located inside the grain and in triple junctions, can reduce the thermal conductivity by effective interface phonon scattering, enhance the electrical conductivity by promoting the abnormal

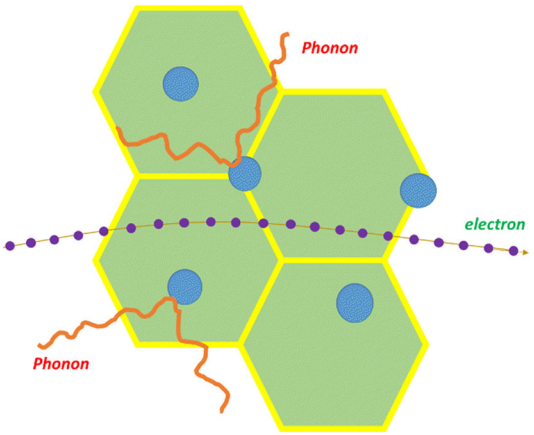

Fig. 3. Phonon–nanoinclusion interaction and electron–nanoinclusion interaction.

grain growth, and thus lead to ninefold enhanced *ZT* value, up to 0.21 at 900 K. According to Fig. 3, oxide nano-inclusions with low thermal conductivity, located inside the grain and in the triple junction, can reduce the thermal conductivity by effective interface phonon scattering, enhance the electrical conductivity by promoting the abnormal grain growth and increase the relative density, and thus lead to the obvious enhancement of the *ZT* value of Nb-$SrTiO_3$.

Furthermore, a colloidal synthesis method combined with spark plasma sintering (SPS) can be used to inexpensively prepare La-doped $SrTiO_3$ nanoparticles that can be used to produce highly stable nanostructured bulk of the La-doped $SrTiO_3$. The nanostructured bulk of the La-doped $SrTiO_3$ exhibited a maximum *ZT* of 0.37 at 973 K, which is one of the highest values reported for doped $SrTiO_3$.[33]

In_2O_3-Based Materials

Recently, it has been reported that Ce-doped In_2O_3[34] is also a promising candidate for high-temperature thermoelectric application, and the dopant of Zn element can further tune the electrical properties.[35] Nanostructured Zn and Ce co-doped In_2O_3-based ceramics were fabricated using co-precipitation and SPS. By decreasing the grain size of In_2O_3-based bulk ceramics, a significant reduction by ~50% in lattice thermal conductivity has been observed in Zn and Ce co-doped In_2O_3-based ceramics with a 50-nm grain size. At the same time, it is interesting that the power factor increases with the decreasing grain size and meanwhile good electric conductivity is kept. As a result, a reported high *ZT* value of 0.4 at 1050 K was achieved.[36]

Moreover, Lan et al. also calculated the "amorphous limit" of thermal conductivity by Cahill's formulation,[37] i.e., about 1.0 $W\,m^{-1}\,K^{-1}$ at 1050 K for In_2O_3-based compounds. According to Fig. 4, the 50-nm grain size is too big to approach this limit, but if it can be brought down to 20 nm (Fig. 4c), the limit of ~1.0 $Wm^{-1}\,K^{-1}$ could be achieved. And thus the *ZT* value can reach up to ~0.7 at 1073 K. Therefore, In_2O_3-based compounds would have promising prospects for high-temperature applications.[36]

p-TYPE OXIDES-BASED THERMOELECTRIC MATERIALS

$Ca_3Co_4O_9$-Based Materials

It is well known that $Ca_3Co_4O_9$ is a misfit layered oxide, which is composed of alternating layers of a distorted CaO-CoO-CaO rock-salt type layer and a CdI_2-type CoO_2 layer stacked along the *c* axis direction.[38,39] These two layers have similar lattice parameters, i.e., *a*, *c*, and β, but different *b* lattice parameters. The first-principle calculations[40] indicated that the electronic structures of the misfit-layered $Ca_3Co_4O_9$ include two-dimensionally dispersive e.g. bands across the Fermi energy, which yields the *p*-type conduction in the rocksalt Ca_2CoO_3 subsystem, while the Fermi energy lies in the crystal-field gap of the *d* states in the CoO_2 layer. Thermoelectric power as well as electrical conductivity varies as a function of carrier concentration, and they have opposite behaviors in their carrier concentration dependence. Some previous experiments revealed that partial substitutions of Ca^{2+} by Bi^{3+}, Gd^{3+} and Na^{+} in $Ca_3Co_4O_9$ could improve thermoelectric properties.[41,42]

Hu et al.[43] prepared *c*-axis-oriented $Ca_3Co_4O_9$ thin films on glass substrate by pulsed laser deposition, and its Seebeck coefficient can be 130 μV/K, which is comparable to those of the single-crystal samples. In single-crystal $(Ca_2CoO_3)_{0.7}CoO_2$ with a $Ca_3Co_4O_9$ structure,[44] thermoelectric power and electrical resistivity are about 240 μV/K and 230 $\mu\Omega$ cm at 973 K, respectively. The large thermoelectric power is mainly related to spin degeneracy, electronic structure, and charge frustration in the vicinity of a Mott metal–insulator transition.[45] For $Ca_3Co_4O_9$/Ag composites,[46] it can be seen that the resistivity of the composite decreases with the addition of Ag over the measured temperature range. The results from scanning electron microscopy (SEM) show that Ag particles have already formed some nano-phases in the $Ca_3Co_4O_9$ matrix, which provides more bypasses for carrier transport. Despite no data about the thermal conductivity $Ca_3Co_4O_9$/Ag composites,[46] with more phonon scattering the κ would be decreased. In addition, nanocrystalline $Ca_3Co_4O_9$ ceramics are also synthesized by using a novel technique combining sol–gel-based electro spinning and SPS. Much smaller grain size and improved texture are observed in the nanofiber-sintered ceramics, resulting in simultaneously enhanced Seebeck coefficient, electric conductivity, and thermal resistivity. Compared with La-doped $Ca_3Co_4O_9$ ceramics synthesized with solid state reaction and spark plasma sintering recently reported,[47] nanofiber-sintered $Ca_3Co_4O_9$ ceramics

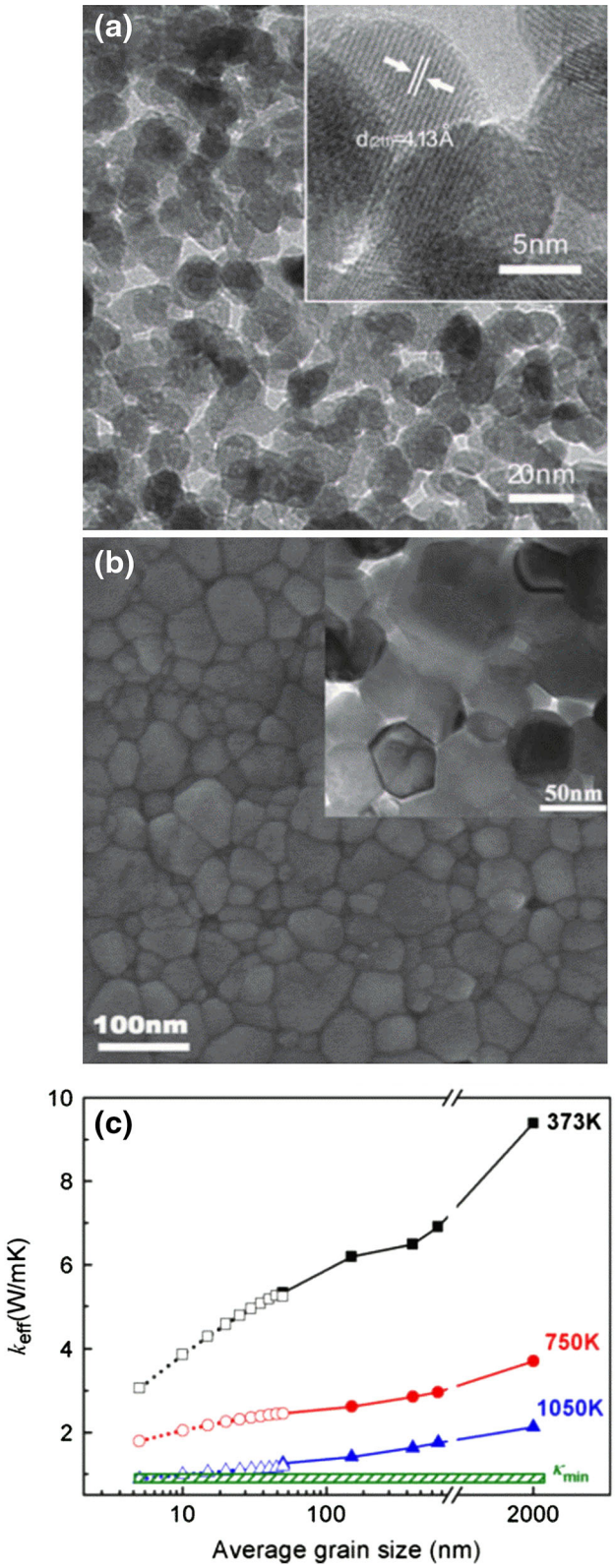

Fig. 4. (a) The TEM image of $In_{1.92}(ZnCe)_{0.08}O_3$nanopowder, (b) the SEM image of 50-nm grain sample, (c) grain size dependence of effective lattice thermal conductivity at different temperatures. Thekminis calculated by theformulation range from 373 to 1050 K (Ref. 36). Copyright (2012) The American Ceramic Society.

even without doping has substantially reduced thermal conductivity, resulting in 55% enhancement of ZT (~0.40 at 975 K).[48]

BiCuSeO-Based Materials

Most recently, BiCuSeO oxyselenide[11,21,49–58] has been reported to exhibit low intrinsic thermal conductivity and tunable electric properties; its highest ZT can be 1.4 at 923 K.[21] BiCuSeO comprises $(Cu_2Se_2)^{2-}$ layers alternately stacked with $(Bi_2O_2)^{2+}$ along the c axis of a tetragonal cell.[59–61] The $(Bi_2O_2)^{2+}$ layers act as charge reservoir, and the conductive $(Cu_2Se_2)^{2-}$ layers provide a conduction pathway for carrier transport. In the entire temperature measurement range, the electrical conductivity is much lower than those of state-of-the-art thermoelectric materials[31,62–65] and about 1.12 S cm^{-1} at room temperature. BiCuSeO has intrinsic low thermal conductivity as low as ~0.40 W m^{-1} K^{-1}at 923 K, but it can be further decreased by nanocomposites. The very low thermal conductivity and high Grüneisen parameter (γ) value of 1.5 in the BiCuSeO system are partially attributed to the increased bond anharmonicity associated with the occurrence of trivalent Bi.[66–68] Combined with the analysis of Young's modulus and Grüneisen parameter (γ) for the BiCuSeO system, other possible reasons include the layered structure since phonons can be confined in the layers and scattered at the layer interfaces,[69] and lower group velocity for the phonons led by the presence of heavy elements.[70] Lan et al. has found that increasing phonon scattering by doping heavy elements could also simultaneously introduce nanocomposites. Many nanodots of 5–10 nm (see inset in Fig. 5) existing in the samples result in highly efficient phonon scattering and thus low thermal conductivity. High σ combined with low κ lead to a significantly enhanced ZT value which shows a maximum of 1.14 at 823 K.[11] Li et al. found that Ca-doped BiCuSeO exhibited a nearly 250-fold electrical conductivity at 300 K and stable low thermal conductivity in comparison with the pure BiCuSeO.[51] The increased boundary density due to the decreased grain size would intensify the scattering of the phonons, thus lowering the lattice thermal conductivity.

The effective mass of ~1.1 m_e was estimated in the undoped BiCuSeO. After doping K, the Fermi level moves deep into the second valence band, and therefore the effective mass of K-doped BiCuSeO is composed of the mixture of heavy and light hole bands, ranging from 0.35 m_e to 0.45 m_e. The increase in the effective mass along with the K doping evidences a non-parabolicity in the light hole band. Since the power factor of BiCuSeO is critically dependent on the effective mass, the similar power factor enhanced behaviors are observed in the K- and Na-doped BiCuSeO.[56,71]

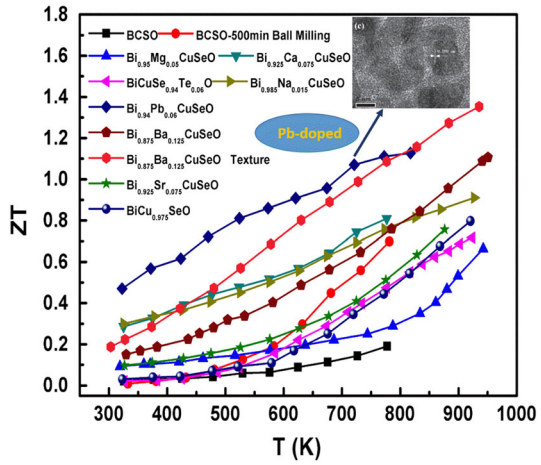

Fig. 5. Recent progress of BiCuSeO (*ZT*). Inset: High-magnification cation transmission electron microscope (TEM) image of $Bi_{1-x}Pb_x$ CuSeO. The fuzzy boundaries and nanodots can be observed in the TEM image (Ref. 12). Copyright (2013) Wiley-VCH, Weinheim.

As a new thermoelectric material, BiCuSeO will play a very important role among oxides in the future, and there are only a few reports based on structure effect. Therefore, the focus on controlling the structure may be the new strategy of developing high performance oxide-based thermoelectric material especially for BiCuSeO.

NiO-Based Materials

Nickel oxide is a *p*-type semiconductor and the undoped one exhibits a cubic rocksalt type crystal structure with a considerable band gap of 3.6–4.0 eV.[72] Although pure NiO is an insulator with extremely low electrical conductivity, Ni^{2+} vacancies can be obtained easily to improve the electrical conductivity.

In recent years, people have paid more and more attention to the thermoelectric properties of NiO. Kadam[73] has examined the σ and S of NiO, which are 10^{-4} S cm^{-1} and 101 μV K^{-1} at 300 K. Poor electrical conductivity limits its application in thermoelectricity. Metallic dopants is a good way to enhance TE properties of NiO. NiO doped with Li still keeps a cubic-type structure of up to 2.42 mol% of Li content, and Li substitution decreased the thermal conductivity resulting in an increase in the thermoelectric figure of merit *ZT* ~0.075 at 1000 K.[14] Although pure Ca-doped NiO single crystals fabricated by floating zone crystal growth technique is an insulator, its electrical properties increase at high temperature due to an increase of vacancies concentration from the Ca^{2+} content.[74]

The use of nanostructures in high-performance thermoelectric materials as a promising approach was also investigated for NiO. At the nanometer scale, quantum confinement effect and surface properties cause changing of both the Fermi level and carriers concentration.[72] The thermal conductivity dramatically decreases NiO samples synthesized nanoparticles using spark plasma sintering and uniaxial hot pressing (~20 Wm^{-1} K^{-1}, RT), comparing NiO single crystal (~50 W m^{-1} K^{-1}, RT).[74] Sher[75] prepared small NiO grains using the method of dispergation, and the thermopower changed quickly though dispergation electrical conductivity did not change much, while obtaining a higher thermoelectric *ZT* (1.5–2 times higher). Furthermore, NiO can be applied as the second phase and leads to the average grain scale of matrix ZnO becoming smaller.[76] More grain boundaries and isolated NiO particles may have an effect on thermoelectric properties. Another study used a hydrogen gas sensor using thermoelectric oxide thin film. They utilized sputtering method for depositing Li-doped NiO and Pt film on single crystal MgO (1 0 0) substrate, which shortened the response time owing to the formation of film structures and crystallization of NiO materials.[77]

Other Oxides: Based Thermoelectric Materials

In addition to those TE oxides discussed above, there are some other materials that have been recently optimized. For example, $CaMnO_3$ has a perovskite-type structure and can be applied as an *n*-type material to high-temperature waste heat recovery in air. The TE properties of $CaMnO_3$ substituted at A or B sites have been widely investigated.[78–82] Among these, a higher *ZT* value of ~0.2 at 1000 K in air was obtained for $Ca_{0.9}Yb_{0.1}MnO_3$ prepared by a conventional solid-state reaction.[59,78] Moreover, the $CaMn_{1-x}Nb_xO_{3-\delta}$ phases (x = 0.02, 0.05, and 0.08) with nano-sized domains characterize the microstructure of the polycrystalline magnets, which act as additional scattering centers affecting the phonons but not the charge carriers. Thus, rotation twins decrease κ due to phonon scattering under conservation of the electronic transport properties, leading to *ZT* = 0.32 at 1060 K for the 2% Nb-doped $CaMnO_3$.[83]

Strategies for Improving the Thermoelectric Performance of Oxide-Based Materials

Recent progress in enhancing the performance of bulk thermoelectric materials have focused on nanostructuring,[70,84–87] all-scale hierarchical architecturing, matrix/precipitate band alignment, and intra-matrix electronic structure engineering.[62] These approaches are now more fully appreciated and well accepted, and they are becoming the prevailing paradigm in the design and optimization of emerging thermoelectric materials. Even though oxide-based thermoelectric materials are very different from alloys in many ways, there are still enough methods for enhancements to work on them.

Nanostructuring

One effective method to produce a structural effect is introducing nanostructure to optimizing

ZT by reducing the thermal conductivity. The lattice thermal conductivity κ_L could be somewhat reduced by increasing phonon scattering through the use of the introduction of rattling centers, mass fluctuation,[88] grain boundaries,[89] complex crystal structures,[64] or nanocomposites.[31] The main issue is to aim for a scattering technique by minimizing electron scattering and maximizing all-length-scale heat carrying phonon scattering.[90,91]

The effect of nanostructured bulk in thermal conductivity can be investigated by the Boltzmann equation. Although it is reported that the electrical properties were enhanced in nanostructured materials through energy filtering, the main focus is to reduce the thermal conductivity to enhance the ZT value. The thermal conductivity of the material can be expressed as:[92,93]

$$k = \frac{k_B}{2\pi^2 v}\left(\frac{k_B T}{\hbar}\right)^3 \int_0^{\theta/T} \frac{\tau_C x^4 e^x}{(e^x - 1)^2} dx \quad (5)$$

where k_B is the Boltzman constant, $\hbar$ is Planck's constant divided by 2π, x is the normalized frequency $\hbar\omega/k_B T$, T is the absolute temperature, and v and θ are the speed of the sound and Debye temperature of the related material. Here, τ_C is the total relaxation time using Matthiessen's rule, given as

$$\tau_c^{-1} = \tau_U^{-1} + \tau_A^{-1} + \tau_{e-ph}^{-1} + \tau_B^{-1} \quad (6)$$

where the total relaxation time include Umklapp phonon–phonon scattering τ_U, point defect scattering τ_A, electron–phonon scattering τ_{e-ph} and boundary scattering τ_B. The electron–phonon scattering contribution is negligible.[94] Assuming the phonon mean-free path (MFP) in nanostructured oxide ceramics is limited to the scale of the nanograin size (l_{gb}),[5] the expression of relaxation time for the grain boundary is

$$\tau_B^{-1} = \frac{v}{l_{gb}} \quad (7)$$

Four kinds of widely researched n-type oxides (ZnO, In_2O_3, $SrTiO_3$, $CaMnO_3$) were investigated by the Boltzmann equation. The Debye temperatures are based on those used in the literature,[95–98] and the speed of sound is estimated via

$$v = \frac{k_B \theta}{\hbar}\left(\frac{6\pi^2}{V}\right)^{1/3} \quad (8)$$

where V is the average volume per atom.

The predictions for bulk oxides are shown in Fig. 6. It can be seen that the agreement is quite good in a wide temperature range. The thermal conductivity of nanostructured bulk oxides are shown in Fig. 6a, and the grain sizes for calculation is 20 nm. It can be seen that the nanograins have a remarkable reduction in thermal conductivity. The nanograins having low thermal conductivity can be explained as below. Although the MFP in oxides is always shorter than the grain size, it varies enormously with frequency as seen in the inset in Fig. 7. The short-wavelength phonons (~Å) are effectively scattered by point defects though a Rayleigh scattering regime. The nanograins of $l_{gb} \sim 20$ nm can scatter the mid- and long-wavelength phonons, which reduces the thermal conductivity. As seen in Fig. 7, the reduction rates of thermal conductivity in the same grain size vary with the oxide. For a simple crystal structure such as ZnO, the thermal conductivity can be reduced by 80%, while the Perovskite-type $CaMnO_3$ has a small reduction ratio such as 15%. The reason is that the complex structure can suppress the thermal conductivity, thus reducing the ratio of the mid- and long-wavelength phonons. Introducing extra defects such as atomic substitution may be more effective in reducing the thermal conductivity in complex structure oxides.

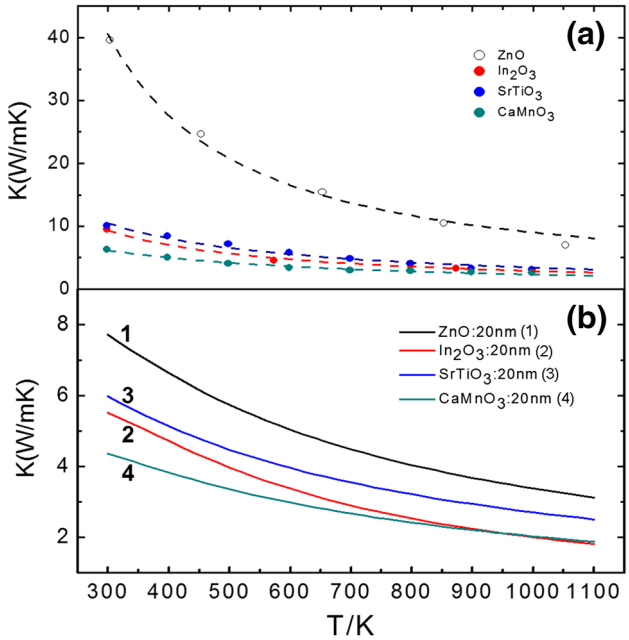

Fig. 6. (a) Experimental (symbols) and calculated (dotted lines) thermal conductivity for four kinds of widely researched n-type undoped oxides. (b) The predicted thermal conductivity of 30-nm grains for the four oxides.

To beat the alloy limit or amorphous limit though nanostructured in oxides is very difficult. The minimum values of the thermal conductivity (k_{min}) can be estimated by Cahill's formulation for noncrystal materials,[99]

$$k_{min} = \left(\frac{\pi}{6}\right)^{1/3} k_b V^{-2/3} \sum v \left(\frac{T}{\theta}\right)^2 \int_0^{\theta/T} \frac{x^3 e^x}{(e^x - 1)^2} dx \quad (9)$$

The k_{min} for the four kinds of oxides is shown in Fig. 8. The striking thing is that k_{min} has the relative high value for the oxides around 1 W m^{-1} K^{-1}.

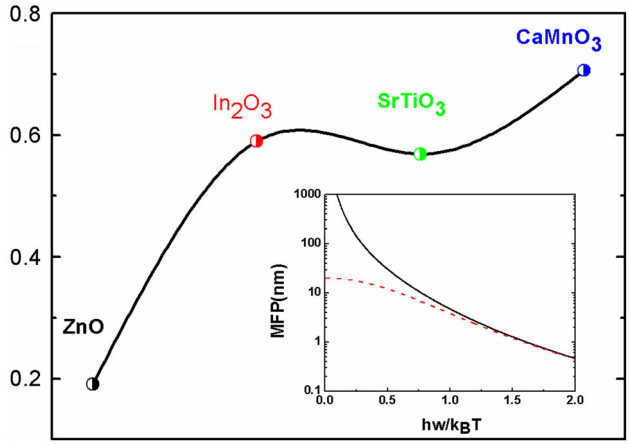

Fig. 7. The reductions of the thermal conductivity of the four kinds of oxides are normalized by the corresponding values of bulk samples. Inset: The chart of MFP varies enormously with frequency.

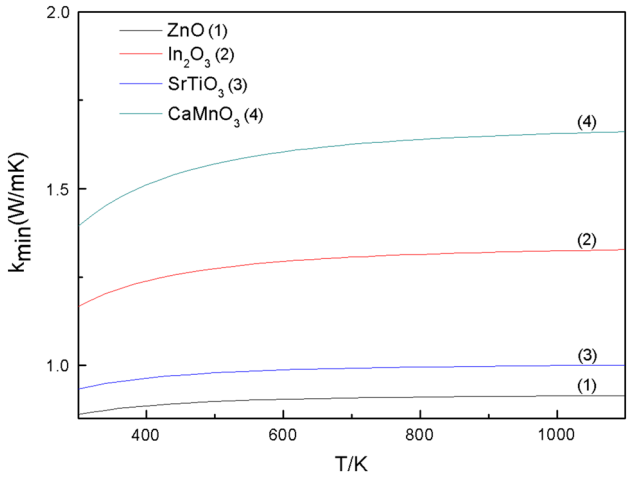

Fig. 8. The k_{min} for ZnO, In_2O_3, $SrTiO_3$, $CaMnO_3$.

The high k_{min} can be ascribed to the strong bonding of the atoms in oxides. The strong bonding of the atoms makes a high speed of sound that increases the k_{min} in Eq. 9. This confirms that nanostructured oxide ceramics cannot achieve low thermal conductivity such as that of the state-of-art alloy system.

Another fact is that the electronic contribution to the thermal conductivity has a comparative value to lattice thermal conductivity at high temperatures for the 30 nm and 200 nm samples. This means that further reducing the lattice thermal conductivity cannot make great improvements in the ZT value.

Low Dimensional Structure

Adding nanoparticles or quantum dots into a material has been successful in reducing κ more effectively than σ as shown in a number of material systems for both n- and p-type semiconductors.[100,101] The quantum dots of the correct size can scatter phonons much more easily than electrons especially for highly doped samples where the electron mean free paths are typically longer than phonon mean free paths. There are a number of examples of materials such as skutterudites where heavy atoms are inserted to fill voids in the lattice in order to have a similar effect at the microscale of the lattice.[64] Superlattices with the electron transport perpendicular to the quantum well and barriers are also good at scattering phonons. If the electrical and thermal transport is along quantum wells then modulation doping can be used to enhance the electrical conductivity.[102] When the dopants are only placed in the barriers which are at higher energy than the quantum well, the carriers fall into the quantum well and are therefore remote from the ionized dopants that created the carriers. By separating the carriers from the dopants, the Coulomb scattering is reduced and the mobility and electrical conductivity increases. The disadvantage of this type of superlattice is that the electrons or holes must quantum-mechanically tunnel through the barriers which also significantly reduces the electrical conductivity to typically 3–4 times lower than bulk material. Finally, nanowires have also demonstrated substantial improvements to ZT. Boukai et al.[103] demonstrated 10-nm-wide Si nanowires which showed enhanced Seebeck coefficients and significantly reduced thermal conductivities compared to bulk Si. The Seebeck coefficient can be maximized using the Cutler and Mott equation

$$S = -\frac{\pi^2}{3q}k_B^2 T\left[\frac{\mathrm{d}\ln(\mu(E)g(E))}{\mathrm{d}E}\right]_{E=E_F} \quad (10)$$

By moving to lower dimensional structures, there is a larger asymmetry in the density of states around the Fermi energy, and the above equation indicates that this increases the Seebeck coefficient. Therefore, the Seebeck coefficient can also be enhanced by choosing systems with lower dimensions.[102] What is more, this occurs along with the Seebeck enhancement described above and so a higher power factor can be created.

The Second Nano-Scale Phase

In addition to low dimensional structure, nanoscale second phase also is an efficient way for improving the overall performance, which can scatter phonons with different wavelengths in the spectrum.[94,104] The second phases can be separated by spinodal decomposition[105] and exsolution[106] to form thermodynamic nanostructures or nanocomposites. These methods have been effectively proved to improve the TE performance of state-of-the-art nonoxide materials, but considering the large difference between oxides and alloys, they would not be appropriate.[15] The very low lattice thermal conductivity of the LAST system[107] was attributed to

the spontaneous and ubiquitous nanoscale precipitation of second phases in the PbTe matrix. After this first observation, *ZT* enhancements by second phases were also observed in the systems STO[32] and ZnO.[12]

Nanograined Boundary

Characteristic phonon–phonon scattering, the Umklapp process,[108] is predominant in the STO bulk single crystal.[15] In contrast, in the case of polycrystalline ceramics, there exists a nonlinear region from room temperature to an elevated temperature above which the temperature dependency is linear. This signifies an additional effect on phonon scattering besides phonon–phonon interactions: grain boundary scattering. Moreover, as the grain size becomes smaller, the nonlinear range becomes wider, which means grain boundary scattering is still effective in restricting phonon propagation at higher temperatures, where the phonon mean free path is even shorter due to enhanced phonon–phonon scattering. If researchers indeed need to enhance *ZT* by the nanograin effect, they need to find revolutionary processing to decrease the size of the crystals below the mean free path of the phonons but pass electrons. Some interesting work has been carried on in In_2O_3.[36]

The nanostructuring approach for oxides has been employed for just the past few years and it has tremendous potential for improvement in TE performance in the future.

Other Optimizations from Structure Effect

Nowadays, as the recent advances in *ZT* based on nanostructures limiting the phonon heat conduction are nearing a fundamental limit, thermal conductivity cannot be reduced below the amorphous limit. Therefore, scientists explored enhancing the Seebeck coefficient through band engineering, such as a distortion of the electronic density of states to increase the Seebeck coefficient.[1,109,110] Combined band engineering with nanostructuring increases S and reduces κ, consequently demonstrating higher performance.

Band structure could be engineered in lead chalcogenides either by modifying the relative energy of the electronic bands through alloying[111–113] or by introducing impurity energy levels which are resonant with the host band through resonant doping[1,114] or both. Among them, resonant impurity doping which leads to profound changes in the electrical properties is an exciting new strategy.[115,116] For example, there is a faster rise of *S* for SnSe when *T* exceeds 500 K, which is attributed to the increasing contribution of the heavy hole Σ band at rising temperatures due to thermal excitations. In addition, considerable bipolar diffusion will occur in compounds with low carrier concentration if the band gap is not large enough, which will significantly deteriorate the high temperature performance.

Even though band engineering is mostly used in metal alloys for thermoelectrics, there are also some dramatic processes for oxide-based thermoelectric materials. For instance, BiCuSeO have a pristine band gap of 0.8 eV, which is low down the overall electrical performance, whereas the BiCuTeO analogue has a band gap of 0.4 eV as reported by Hiramatsu et al.[117] After recognizing a solid solution study of the Se/Te system by Barreteau,[49] researchers observed that transport properties of BiCuSeO can be enhanced through Te properly replacing Se. Generalizing this method for other oxides, coupled with potential low thermal conductivity, and a successful route to achieve high thermoelectric performance would be ultimately achieved.

Finally, how can we obtain higher *ZT* values? The possible ways are first, introduce extra defects such as atomic substitution or oxygen vacancies from growth processes in oxygen-deficient environment to reduce thermal conductivity at high temperature. These randomly distributed defects and clustered vacancies could provide effective strong phonon scattering, and result in large thermal conductivity suppression.[118] The randomly distributed defects and clustered vacancies are much more effectively in short-wavelength phonon scatter which dominate scattering regime at high temperature.[94] It may be more effective in reducing thermal conductivity as compared to the reduction from the nanograin size effects at high temperature, which could be more beneficial in enhancing *ZT* of oxygen-contained complex oxides.

Second, construct porous microstructures to reduce thermal conductivity in oxides ceramics. Higher power factor and lower thermal conductivity could be desirable in these porous oxides ceramics. In the Nb-doped $CaMnO_3$ porous ceramics (relative density $\sim$ 68–81%), the thermal conductivity can be about 0.73–0.91 $W\,m^{-1}\,K^{-1}$ at 800 K.[82] Our experiments also reveal that the thermal conductivity can be 1.3 $W\,m^{-1}\,K^{-1}$ at 973 K in the Gd-doped $CaMnO_3$ (relative density $\sim$ 85%).[9] If we can improve the electrical conductivity by the interconnections between the crystallites, *ZT* could be enhanced effectively.

Third, achieve low dimensional oxides structures. In the $SrTiO_3$ superlattice, *ZT* values can be $\sim$2.4, which is 24 times larger than that of the $SrTiO_3$ bulk.[119] High-density carrier electrons are localized within a unit cell layer thickness of $SrTiO_3$ at the hetero-interface, which leads to a giant Seebeck coefficient ($\sim$850 $\mu V\,K^{-1}$), thus resulting in greatly enhanced *ZT*. In the Bi_2Te_3/Sb_2Te_3 superlattices, *ZT* $\sim$2.4 can also be obtained at 300 K.[69] These experimental results indicate that *ZT* values can be further enhanced by using low-dimensional structures.

SUMMARY

Oxide-based thermoelectric materials based on structural effect have been reviewed as potential candidate *n*- and *p*-type materials. Structural effect is a very important method to modify thermoelectric materials' performance. Nonetheless, most oxide-based thermoelectric materials have only been studied by traditional ways such as doping. *ZT* enhancements by structural effect especially nanostructure is the next promising strategy. Nanostructuring techniques leads to phonon scattering at interfaces and therefore achieve low thermal conductivity, combined with band engineering which alters electronic configuration and DOS to optimize the thermopower and electron–phonon interaction in a way to regulate power factor. More developments for oxide-based thermoelectric materials and more and more thermoelectric applications characterized by thermal and chemical stability would be obtained in the future.

ACKNOWLEDGEMENTS

This work was financially supported by the Ministry of Science & Technology of China through a 973-Project, under Grant No. 2013CB632506, NSF of China under Grant No. 51025205 and 11234012, and Specialized Research Fund for the Doctoral Program of Higher Education, under Grant No. 20120002110006.

REFERENCES

1. J.P. Heremans, V. Jovovic, E.S. Toberer, A. Saramat, K. Kurosaki, A. Charoenphakdee, S. Yamanaka, and G.J. Snyder, *Science* 321, 554 (2008).
2. M. Scheele, N. Oeschler, K. Meier, A. Kornowski, C. Klinke, and H. Weller, *Adv. Funct. Mater.* 19, 3476 (2009).
3. W. Liu, X. Tan, K. Yin, H. Liu, X. Tang, J. Shi, Q. Zhang, and C. Uher, *Phys. Rev. Lett.* 108, 166601 (2012).
4. Q. Hou, D. Liang, X. Feng, W. Zhao, Y. Chen, and Y. He, *Mod. Phys. Lett. B* 21, 1447 (2007).
5. A. Minnich, H. Lee, X. Wang, G. Joshi, M. Dresselhaus, Z. Ren, G. Chen, and D. Vashaee, *Phys. Rev. B* 80, 155327 (2009).
6. L.D. Zhao, S.H. Lo, Y. Zhang, H. Sun, G. Tan, C. Uher, C. Wolverton, V.P. Dravid, and M.G. Kanatzidis, *Nature* 508, 373 (2014).
7. A. Nag and V. Shubha, *J. Electron. Mater.* 43, 962 (2014).
8. Y.-H. Lin, C.-W. Nan, Y. Liu, J. Li, T. Mizokawa, and Z. Shen, *J. Am. Ceram. Soc.* 90, 132 (2007).
9. J. Lan, Y.H. Lin, H. Fang, A. Mei, C.W. Nan, Y. Liu, S. Xu, and M. Peters, *J. Am. Ceram. Soc.* 93, 2121 (2010).
10. T. Okuda, K. Nakanishi, S. Miyasaka, and Y. Tokura, *Phys. Rev. B* 63, 113104 (2001).
11. J.L. Lan, Y.C. Liu, B. Zhan, Y.H. Lin, B. Zhang, X. Yuan, W. Zhang, W. Xu, and C.W. Nan, *Adv. Mater.* 25, 5086 (2013).
12. P. Jood, R.J. Mehta, Y. Zhang, G. Peleckis, X. Wang, R.W. Siegel, T. Borca-Tasciuc, S.X. Dou, and G. Ramanath, *Nano Lett.* 11, 4337 (2011).
13. D. Bérardan, E. Guilmeau, A. Maignan, and B. Raveau, *Solid State Commun.* 146, 97 (2008).
14. W. Shin and N. Murayama, *Jpn. J. Appl. Phys. B* 38, L1336 (1999).
15. K. Koumoto, Y. Wang, R. Zhang, A. Kosuga, and R. Funahashi, *Annu. Rev. Mater. Res.* 40, 363 (2010).
16. H. Ohta, K. Sugiura, and K. Koumoto, *Inorg. Chem.* 47, 8429 (2008).
17. J. He, Y. Liu, and R. Funahashi, *J. Mater. Res.* 26, 1762 (2011).
18. K. Koumoto, I. Terasaki, and R. Funahashi, *MRS Bull.* 31, 206 (2006).
19. M. Ohtaki, Kyushu University Global COE Program, *Novel Carbon Resour. Sci. Newslett.* 3 (2010).
20. I. Terasaki, Y. Sasago, and K. Uchinokura, *Phys. Rev. B* 56, R12685 (1997).
21. J. Sui, J. Li, J. He, Y.-L. Pei, D. Berardan, H. Wu, N. Dragoe, W. Cai, and L.-D. Zhao, *Energ. Environ. Sci.* 6, 2916 (2013).
22. M. Ohtaki, K. Araki, and K. Yamamoto, *J. Electron. Mater.* 38, 1234 (2009).
23. M. Ohtaki, T. Tsubota, K. Eguchi, and H. Arai, *J. Appl. Phys.* 79, 1816 (1996).
24. Z.-H. Wu, H.-Q. Xie, and Y.-B. Zhai, *Appl. Phys. Lett.* 103, 243901 (2013).
25. D. Khanal, J.W. Yim, W. Walukiewicz, and J. Wu, *Nano Lett.* 7, 1186 (2007).
26. C. Wang, Y. Wang, G. Zhang, C. Peng, and G. Yang, *Phys. Chem. Chem. Phys.* 16, 3771 (2014).
27. N. Schäuble, B.E. Süess, S. Populoh, A. Weidenkaff, and M.H. Aguirre, eds., *A Morphology Study on Thermoelectric Al-Substituted ZnO. 9th European Conference on Thermoelectrics: ECT2011* (Melville, NY: AIP Publishing, 2012).
28. P. Jood, R.J. Mehta, Y. Zhang, T. Borca-Tasciuc, S.X. Dou, D.J. Singh, and G. Ramanath, *RSC Advances* 4, 6363 (2014).
29. S. Ohta, T. Nomura, H. Ohta, and K. Koumoto, *J. Appl. Phys.* 97, 034106 (2005).
30. H. Suzuki, H. Bando, Y. Ootuka, I.H. Inoue, T. Yamamoto, K. Takahashi, and Y. Nishihara, *J. Phys. Soc. Jpn.* 65, 1529 (1996).
31. M.S. Dresselhaus, G. Chen, M.Y. Tang, R. Yang, H. Lee, D. Wang, Z. Ren, J.P. Fleurial, and P. Gogna, *Adv. Mater.* 19, 1043 (2007).
32. N. Wang, H. Chen, H. He, W. Norimatsu, M. Kusunoki, and K. Koumoto, *Sci. Rep.* 3 (2013).
33. K. Park, J.S. Son, S.I. Woo, K. Shin, M.-W. Oh, S.-D. Park, and T. Hyeon, *J. Mater. Chem. A* 2, 4217 (2014).
34. B. Cheng, H. Fang, J. Lan, Y. Liu, Y.-H. Lin, and C.-W. Nan, *J. Am. Ceram. Soc.* 94, 2279 (2011).
35. Y. Liu, Y.H. Lin, W. Xu, B. Cheng, J. Lan, D. Chen, H. Zhu, and C.W. Nan, *J. Am. Ceram. Soc.* 95, 2568 (2012).
36. J. Lan, Y.H. Lin, Y. Liu, S. Xu, and C.W. Nan, *J. Am. Ceram. Soc.* 95, 2465 (2012).
37. D.G. Cahill, S.K. Watson, and R.O. Pohl, *Phys. Rev. B* 46, 6131 (1992).
38. A. Masset, C. Michel, A. Maignan, M. Hervieu, O. Toulemonde, F. Studer, B. Raveau, and J. Hejtmanek, *Phys. Rev. B.* 62, 166 (2000).
39. Y. Morita, J. Poulsen, K. Sakai, T. Motohashi, T. Fujii, I. Terasaki, H. Yamauchi, and M. Karppinen, *J. Solid State Chem.* 177, 3149 (2004).
40. R. Asahi, J. Sugiyama, and T. Tani, *Phys. Rev. B* 66, 155103 (2002).
41. G. Xu, R. Funahashi, M. Shikano, I. Matsubara, and Y. Zhou, *Appl. Phys. Lett.* 80, 3760 (2002).
42. G. Xu, R. Funahashi, M. Shikano, Q. Pu, and B. Liu, *Solid State Commun.* 124, 73 (2002).
43. Y. Hu, E. Sutter, W. Si, and Q. Li, *Appl. Phys. Lett.* 87, 171912 (2005).
44. M. Shikano and R. Funahashi, *Appl. Phys. Lett.* 82, 1851 (2003).
45. O. Motrunich and P.A. Lee, *Phys. Rev. B* 69, 214516 (2004).
46. P.-H. Xiang, Y. Kinemuchi, H. Kaga, and K. Watari, *J. Alloys Compd.* 454, 364 (2008).
47. Y.-H. Lin, J. Lan, Z. Shen, Y. Liu, C.-W. Nan, and J.-F. Li, *Appl. Phys. Lett.* 94, 072107 (2009).
48. T. Yin, D. Liu, Y. Ou, F. Ma, S. Xie, J.-F. Li, and J. Li, *J. Phys. Chem. C* 114, 10061 (2010).
49. C. Barreteau, D. Bérardan, L. Zhao, and N. Dragoe, *J. Mater. Chem. A* 1, 2921 (2013).
50. J.-L. Lan, B. Zhan, Y.-C. Liu, B. Zheng, Y. Liu, Y.-H. Lin, and C.-W. Nan, *Appl. Phys. Lett.* 102, 123905 (2013).

51. F. Li, T.-R. Wei, F. Kang, and J.-F. Li, *J. Mater. Chem. A* 1, 11942 (2013).
52. J. Li, J. Sui, C. Barreteau, D. Berardan, N. Dragoe, W. Cai, Y. Pei, and L.-D. Zhao, *J. Alloys Compd.* 551, 649 (2013).
53. Y. Liu, J. Lan, W. Xu, Y. Liu, Y.L. Pei, B. Cheng, D.B. Liu, Y.H. Lin, and L.D. Zhao, *Chem. Commun. (Camb.)* 49, 8075 (2013).
54. S.D.N. Luu and P. Vaqueiro, *J. Mater. Chem. A* 1, 12270 (2013).
55. L. Pan, D. Bérardan, L. Zhao, C.L. Barreteau, and N. Dragoe, *Appl. Phys. Lett.* 102, 023902 (2013).
56. D. Sun Lee, T.-H. An, M. Jeong, H.-S. Choi, Y. Soo Lim, W.-S. Seo, C.-H. Park, C. Park, and H.-H. Park, *Appl. Phys. Lett.* 103, 232110 (2013).
57. W. Xu, Y. Liu, L.-D. Zhao, P. An, Y.-H. Lin, A. Marcelli, and Z. Wu, *J. Mater. Chem. A* 1, 12154 (2013).
58. D. Zou, S. Xie, Y. Liu, J. Lin, and J. Li, *J. Mater. Chem. A* 1, 8888 (2013).
59. C. Wiebe, J. Greedan, J. Gardner, Z. Zeng, and M. Greenblatt, *Phys. Rev. B* 64, 064421 (2001).
60. A. Kusainova, P. Berdonosov, L. Akselrud, L. Kholodkovskaya, V. Dolgikh, and B. Popovkin, *J. Solid State Chem.* 112, 189 (1994).
61. A. Richard, J. Russell, A. Zakutayev, L. Zakharov, D. Keszler, and J. Tate, *J. Solid State Chem.* 187, 15 (2012).
62. L.-D. Zhao, V.P. Dravid, and M.G. Kanatzidis, *Energ. Environ. Sci.* 7, 251 (2014).
63. J.R. Sootsman, D.Y. Chung, and M.G. Kanatzidis, *Angew. Chem. Int. Ed. Engl.* 48, 8616 (2009).
64. G.J. Snyder and E.S. Toberer, *Nat. Mater.* 7, 105 (2008).
65. J.P. Heremans, C.M. Thrush, and D.T. Morelli, *Phys. Rev. B* 70, 115334 (2004).
66. D. Sanditov and V. Belomestnykh, *Tech. Phys.* 56, 1619 (2011).
67. M. Roufosse and P. Klemens, *Phys. Rev. B* 7, 5379 (1973).
68. E.J. Skoug, J.D. Cain, and D.T. Morelli, *Appl. Phys. Lett.* 98, 261911 (2011).
69. R. Venkatasubramanian, E. Siivola, T. Colpitts, and B. O'quinn, *Nature* 413, 597 (2001).
70. J.-F. Li, W.-S. Liu, L.-D. Zhao, and M. Zhou, *NPG Asia Mater.* 2, 152 (2010).
71. J. Li, J. Sui, Y. Pei, X. Meng, D. Berardan, N. Dragoe, W. Cai, and L.-D. Zhao, *J. Mater. Chem. A* 2, 4903 (2014).
72. S. Walia, S. Balendhran, H. Nili, S. Zhuiykov, G. Rosengarten, Q.H. Wang, M. Bhaskaran, S. Sriram, M.S. Strano, and K. Kalantar-zadeh, *Prog. Mater Sci.* 58, 1443 (2013).
73. P. Patil and L. Kadam, *Appl. Surf. Sci.* 199, 211 (2002).
74. L. Cieniek, J. Kusinski, G. Petot-Ervas, and C. Petot, *J. Microsc.* 237, 329 (2010).
75. E. Sher, eds., *Thermoelectric Properties of Transition Metal Oxides (NiO and TiO_2) in a Finely Dispersgated State. XX International Conference on Thermoelectrics, 2001. Proceedings ICT 2001* (Piscataway, NJ: IEEE, 2001).
76. K. Park, J. Seong, and G.H. Kim, *J. Alloys Compd.* 473, 423 (2009).
77. M. Matsumiya, F. Qiu, W. Shin, N. Izu, N. Murayama, and S. Kanzaki, *Thin Solid Films* 419, 213 (2002).
78. D. Flahaut, T. Mihara, R. Funahashi, N. Nabeshima, K. Lee, H. Ohta, and K. Koumoto, *J. Appl. Phys.* 100, 084911 (2006).
79. M. Ohtaki, H. Koga, T. Tokunaga, K. Eguchi, and H. Arai, *J. Solid State Chem.* 120, 105 (1995).
80. Y. Wang, Y. Sui, and W. Su, *J. Appl. Phys.* 104, 093703 (2008).
81. G. Xu, R. Funahashi, Q. Pu, B. Liu, R. Tao, G. Wang, and Z. Ding, *Solid State Ionics* 171, 147 (2004).
82. L. Bocher, M. Aguirre, D. Logvinovich, A. Shkabko, R. Robert, M. Trottmann, and A. Weidenkaff, *Inorg. Chem.* 47, 8077 (2008).
83. L. Bocher, R. Robert, M.H. Aguirre, S. Malo, S. Hébert, A. Maignan, and A. Weidenkaff, *Solid State Sci.* 10, 496 (2008).
84. C.J. Vineis, A. Shakouri, A. Majumdar, and M.G. Kanatzidis, *Adv. Mater.* 22, 3970 (2010).
85. J.P. Heremans, M.S. Dresselhaus, L.E. Bell, and D.T. Morelli, *Nat. Nanotechnol.* 8, 471 (2013).
86. W. Liu, X. Yan, G. Chen, and Z. Ren, *Nano Energy* 1, 42 (2012).
87. P. Pichanusakorn and P. Bandaru, *Mat. Sci. Eng. R* 67, 19 (2010).
88. E. GroB, M. Riffel, and U. Stohrer, *J. Mater. Res.* 10, 35 (1995).
89. K.F. Hsu, S. Loo, F. Guo, W. Chen, J.S. Dyck, C. Uher, T. Hogan, E.K. Polychroniadis, and M.G. Kanatzidis, *Science* 303, 818 (2004).
90. K. Biswas, J. He, I.D. Blum, C.I. Wu, T.P. Hogan, D.N. Seidman, V.P. Dravid, and M.G. Kanatzidis, *Nature* 489, 414 (2012).
91. A. Majumdar, *Science* 303, 777 (2004).
92. N. Mingo, *Phys. Rev. B* 68, 113308 (2003).
93. B. Abeles, *Phys. Rev.* 131, 1906 (1963).
94. W. Kim, J. Zide, A. Gossard, D. Klenov, S. Stemmer, A. Shakouri, and A. Majumdar, *Phys. Rev. Lett.* 96, 045901 (2006).
95. H. Landolt-Bornstein, W. Axford, L.H. Aller, and P. Biermann, *Numerical Data and Functional Relationships in Science and Technology: Group VI: Astronomy Astrophysics and Space Research* (Berlin: Springer, 1982).
96. Z. Ovadyahu and Y. Imry, *Phys. Rev. B* 24, 7439 (1981).
97. M. Ahrens, R. Merkle, B. Rahmati, and J. Maier, *Phys. B* 393, 239 (2007).
98. A. Srivastava and N. Gaur, *J. Phys.: Condens. Matter* 21, 096001 (2009).
99. M.P. Zaitlin and A. Anderson, *Phys. Rev. B* 12, 4475 (1975).
100. T. Harman, P. Taylor, M. Walsh, and B. LaForge, *Science* 297, 2229 (2002).
101. T. Harman, M. Walsh, and G. Turner, *J. Electron. Mater.* 34, L19 (2005).
102. D.J. Paul, *ICT - Energy Concepts Towards Zero-Power Information and Communication*, ed. G. Fagas (Rijeka, Croatia: InTech Europe, 2014). doi:10.5772/57092.
103. A.I. Boukai, Y. Bunimovich, J. Tahir-Kheli, J.-K. Yu, W.A. Goddard Iii, and J.R. Heath, *Nature* 451, 168 (2008).
104. S.N. Girard, J. He, C. Li, S. Moses, G. Wang, C. Uher, V.P. Dravid, and M.G. Kanatzidis, *Nano Lett.* 10, 2825 (2010).
105. J. Androulakis, C.-H. Lin, H.-J. Kong, C. Uher, C.-I. Wu, T. Hogan, B.A. Cook, T. Caillat, K.M. Paraskevopoulos, and M.G. Kanatzidis, *J. Am. Chem. Soc.* 129, 9780 (2007).
106. Q. Zhang, J. He, T. Zhu, S. Zhang, X. Zhao, and T. Tritt, *Appl. Phys. Lett.* 93, 102109 (2008).
107. B.A. Cook, M.J. Kramer, J.L. Harringa, M.K. Han, D.Y. Chung, and M.G. Kanatzidis, *Adv. Funct. Mater.* 19, 1254 (2009).
108. S. Raghavan, H. Wang, R.B. Dinwiddie, W.D. Porter, and M.J. Mayo, *Scripta Mater.* 39, 1119 (1998).
109. G. Tan, L.D. Zhao, F. Shi, J.W. Doak, S.H. Lo, H. Sun, C. Wolverton, V.P. Dravid, C. Uher, and M.G. Kanatzidis, *J. Am. Chem. Soc.* (2014).
110. Y. Pei, H. Wang, and G.J. Snyder, *Adv. Mater.* 24, 6125 (2012).
111. Y. Pei, X. Shi, A. LaLonde, H. Wang, L. Chen, and G.J. Snyder, *Nature* 473, 66 (2011).
112. S.N. Girard, J. He, X. Zhou, D. Shoemaker, C.M. Jaworski, C. Uher, V.P. Dravid, J.P. Heremans, and M.G. Kanatzidis, *J. Am. Chem. Soc.* 133, 16588 (2011).
113. Y. Pei, A.D. LaLonde, N.A. Heinz, X. Shi, S. Iwanaga, H. Wang, L. Chen, and G.J. Snyder, *Adv. Mater.* 23, 5674 (2011).
114. Q. Zhang, H. Wang, W. Liu, H. Wang, B. Yu, Q. Zhang, Z. Tian, G. Ni, S. Lee, and K. Esfarjani, *Energy Environ. Sci.* 5, 5246 (2012).
115. J.P. Heremans, B. Wiendlocha, and A.M. Chamoire, *Energy Environ. Sci.* 5, 5510 (2012).
116. S. Nemov and Y.I. Ravich, *Phys. Usp.* 41, 735 (1998).
117. H. Hiramatsu, H. Yanagi, T. Kamiya, K. Ueda, M. Hirano, and H. Hosono, *Chem. Mater.* 20, 326 (2008).
118. C. Yu, M.L. Scullin, M. Huijben, R. Ramesh, and A. Majumdar, *Appl. Phys. Lett.* 92, 191911 (2008).
119. H. Ohta, S. Kim, Y. Mune, T. Mizoguchi, K. Nomura, S. Ohta, T. Nomura, Y. Nakanishi, Y. Ikuhara, and M. Hirano, *Nat. Mater.* 6, 129 (2007).